Phase Change Materials: from crystal structures to kinetics

R. Detemple[1], H. Dieker[1], J. Kalb[1,2,*], M. Luo[1], F. Spaepen[2], C. Steimer[1],
D. Wamwangi[1], H.W. Wöltgens[1], S. Ziegler[1] and M. Wuttig[1]
[1]Department of Physics, Physics of New Materials, Aachen University of Technology (RWTH Aachen), Germany
[2]Division of Engineering and Applied Sciences, Harvard University, Cambridge, MA, USA

ABSTRACT

Phase change materials are characterized by a structural transition that is accompanied by a pronounced change of properties. We have recently focused our efforts to understand and identify suitable phase change materials onto the identification of suitable structures and the detailed study of crystallization kinetics. For a large number of samples it could be shown that only those samples with a particular group of structures enabled phase change recording. All materials that showed the required optical contrast between the amorphous and crystalline state had cubic or near-cubic crystal structures, while materials based upon tetrahedral crystal structures showed insufficient contrast. The different behavior of these two groups of materials could be explained in part by density functional theory which has been employed to determine the density of states, the band structure and the total energy for different structures of ternary alloys containing Cu, Ag, Au, Ga, In, Ge, Sn, As, Sb and Te. While these results help to understand which stoichiometries are suitable for phase change recording and why certain structures are frequently encountered, the question still remains to be solved what characterizes the kinetics of crystallization for the different classes of phase change alloys. Ex-situ atomic force microscopy in combination with a high-precision furnace has been employed for a systematic study of crystallization kinetics of sputtered amorphous $Ag_{0.055}In_{0.065}Sb_{0.59}Te_{0.29}$, $Ge_4Sb_1Te_5$, and $Ge_2Sb_2Te_5$ thin films used for optical data storage. Direct observation of crystals enabled us to establish the temperature dependence of the crystal nucleation rate and crystal growth velocity around 150° C. While these alloys exhibited similar crystal growth characteristics, the crystal nucleation behavior of $Ag_{0.055}In_{0.065}Sb_{0.59}Te_{0.29}$ differed significantly from that of $Ge_4Sb_1Te_5$ and $Ge_2Sb_2Te_5$. These observations provide an explanation for the different re-crystallization mechanisms observed upon laser-heating of amorphous marks.

Keywords: Optical disk, phase change recording, crystal structure, density functional theory calculations, valence electrons distribution, re-crystallization mechanism, crystal growth velocity, crystal nucleation rate

1. INTRODUCTION

The goal of this work is to determine design rules for suitable phase change alloys, which should help to *predict* important properties like the optical contrast between the amorphous and crystalline phase or the recrystallization mechanism. Therefore, in Section 2 of this manuscript a criterion is presented that phase change alloys have to fulfill in order to work. It is shown how stoichiometry and crystal structure determine optical properties of phase change alloys. In the long run, we would like to predict which alloy stochiometry has desired properties, both in terms of optical or electrical contrast, melting temperature, and also crystallization kinetics, which are crucial for successful applications, too. Therefore, in Section 3 a study of the recrystallization mechanism of different alloys is presented. We would like to be able to predict the recrystallization mechanism as a function of stoichiometry in the long run.

2. STOCHIOMETRY, CRYSTAL STRUCTURE AND OPTICAL PROPERTIES

Previously, it has been shown that alloys containing Ag, In, Sb and Te are particularly suitable for phase change recording[1]. Frequently, alloys of these elements decompose[2] upon prolonged heating into $AgInTe_2$ and $AgSbTe_2$. Hence, we have prepared alloy films of these two materials and investigated their structural and optical properties; analyzed their recording behavior and performed bandstructure calculations of the ground states using density functional theory (DFT) to understand the measured properties.

* Speaker and author to whom correspondence should be sent: kalb [at] deas.harvard.edu

In a first series of experiments, laser induced initial crystallization of as-deposited amorphous films (thickness: 50nm), which were deposited on Si wafers and glass slides by thermal evaporation, was observed in a static tester. In these experiments a laser beam with a focus size of 0.46 μm at the sample position was utilized where the laser power was varied between 0 and 30 mW, and the pulse length ranged between 10 ns and 1 s. On films of both compositions, ablation was observed for long pulses and/or high powers. Ablative hole formation leading to a decrease of film reflectance was confirmed by atomic force microscopy. However, an increase of film reflectance, which is characteristic for crystallization was only observed for the $AgSbTe_2$ films, while no such reflectance change was observed for the $AgInTe_2$ films no matter how long and/or intense the laser beam was. *This either implies that crystallization was not possible or that the change in reflectance for this material is smaller than the smallest measurable reflectance change of our tester, which is smaller than 0.01*. However, it is known from x-ray diffraction (XRD) and measurements of the electrical film resistance[3] that furnace crystallization *is* possible for $AgInTe_2$. Therefore, we conclude that *laser* induced crystallization should be possible for $AgInTe_2$ films as well, which indicates that this alloy might only show weak optical contrast between the amorphous and crystalline state.

The lack of optical contrast for $AgInTe_2$ was confirmed by optical spectroscopy and spectroscopic ellipsometry. The measured data were reproduced by modeling the dielectric function of both $AgInTe_2$ and $AgSbTe_2$. The two most important results of this analysis were a much higher absorption of the $AgSbTe_2$ films as compared with the $AgInTe_2$ films and a larger change of optical properties between the amorphous and crystalline state for $AgSbTe_2$ than for $AgInTe_2$. This is displayed in Fig. 1, where the calculated change of normalized reflectance for a 60 nm thin film on glass as a function of the wavelength is plotted for $AgInTe_2$ and $AgSbTe_2$ based upon the dielectric functions determined for the two states of the two alloys. The experimentally observed small reflectance change for $AgInTe_2$ is in good agreement with the corresponding value calculated from the dielectric functions for both phases. It can hence be concluded that it is the *missing* optical contrast between the amorphous and crystalline state of the $AgInTe_2$ sample which renders it useless for rewritable optical data storage. To understand this phenomenon, the density and thickness change upon furnace crystallization were determined for both alloys by x-ray reflectivity measurements. The corresponding data are displayed in Fig. 2, where all values have been normalized with respect to the density and thickness of the as-deposited film. Crystallization occurs around 100° C and is accompanied by a reduction of film thickness and a corresponding increase of density by 1.4% for $AgInTe_2$ and by 4.8% for $AgSbTe_2$. Clearly speaking, the $AgSbTe_2$ alloy, which had shown the large optical contrast, also shows a large density contrast. On the other hand, the $AgInTe_2$ alloy, which had shown the small optical contrast, shows a small density contrast. *This suggests that there is a clear correlation between the magnitude of density change and optical contrast.*

To understand the different behavior of the two alloys further, XRD measurements were performed[3] on samples, which were furnace annealed at 220° C, which is sufficiently above the crystallization temperature. The analysis of the spectrum[3] reveals that $AgInTe_2$ crystallizes into the chalcopyrite structure, whose bonding is based on sp^3-hybridization, while $AgSbTe_2$ crystallizes into the rocksalt structure, which is based on p-bonding. Since the atomic radii of In and Sb are similar (their atomic number only differs by two), the change of ground state structure from chalcopyrite to rocksalt cannot be ascribed to a difference in atomic radius *but must have an electronic origin and may be related to the number of available valence electrons.*

To understand this point further, we have performed density functional theory (DFT) calculations for the two crystallographic arrangements employing the generalized gradient approximation[4], using the FLEUR code based on the full-potential linearized augmented planewave method[5]. The total energy *E* per atom for all possible combinations is shown in Fig. 3 as a function of lattice parameter *a*. Figure 3 shows calculations where Ag was replaced by Au, but we got qualitatively the same results for Ag- and Au-based alloys. This is because Ag and Au are iso-electronic, i.e. they exhibit the same valence electron configuration. Figure 3 shows that the chalcopyrite structure is more stable for $AuInTe_2$, while the rocksalt structure is more stable for $AuSbTe_2$. Calculated crystal structure and lattice parameter *a* for the stable structure at the energy minimum are in agreement with XRD measurements for both alloys[3,6,7].

We employed DFT also to calculate the density of valence electrons[7]. Figure 4 (A) shows the 001 plane of $AuSbTe_2$ and indicates p-bonding for the rocksalt structure. Figure 4 (B) shows the (110) plane of $AuInTe_2$ and shows sp^3-bonding for the chalcopyrite structure. On average, the number of valence electrons is 4 for $AuInTe_2$ (the d shell is assumed to be full and is *not* counted when determining the average number of valence electrons). In this case the binding sp^3-orbitals

are filled, but the antibonding orbitals are empty. For $AuSbTe_2$, the average number of valence electrons is 4.5. Therefore, our results imply that *increasing the number of valence electrons from 4 to 4.5 destabilizes the chalcopyrite structure and favors the rocksalt structure due to filling of antibonding sp^3-orbitals.* For the rocksalt structure, the ideal situation is that each atom provides three p-electrons for p-bonding, so that the number of valence electrons (including s and p electrons) would be 5. In this case, only the binding p-orbitals are filled. We may pose the question which other alloys prefer the rocksalt structure over the chalcopyrite structure: These materials may be suitable for phase change recording because the rocksalt structure may imply a large density change and therefore a large change in optical properties. We may expect the transition between sp^3- and p-bonding somewhere between a valence electron number of 4 and 4.5.

Figure 5 is a plot of the energy difference between chalcopyrite and rocksalt structure per atom as a function of the average valence electron number N_{sp} for various ternary alloys obtained from DFT calculations. It is interesting to note that the energy difference between rocksalt and chalcopyrite structure is almost the same for isoelectronic compounds. When N_{sp} =4, the alloys prefer sp3-bonding, and therefore, the chalcopyrite structure. If N_{sp} increases, ΔE is decreases. From this simple graphic representation we find that for $N_{sp} >\sim 4.1$, p-bonding is prefered, and therefore, the rocksalt structure is prefered over the chalcopyrite structure. Even though this result does not imply that those alloys will have a rocksalt structure since other crystalline phases might even have a lower energy, we can exclude the chalcopyrite structure. Replacing In by Sb in Figs. 1-4 increased N_{sp} from 4 to 4.5 and therefore the crystal structure from chalcopyrite to rocksalt. Hence, we expect that materials with $N_{sp} >\sim 4.1$ are suitable phase change alloys, because the rocksalt structure may imply a large difference in density and therefore a large optical contrast between amorphous and crystalline phase. Indeed, we have applied this criterion successfully to $AgSnTe_2$, whose N_{sp} is 4.25. In agreement with the prediction, our experiments have shown a high optical contrast between amorphous and crystalline phase, so this alloy would be suitable for phase change recording. *This is the first time a phase change material has been designed by DFT calculations rather than trial and error preparation procedures.*

Table I shows some successful and unsuccessful phase change alloys taken from various publications listed in Ref. 7. 'Successful' means that the material has sufficient optical contrast and can crystallize rapidly. Apparently our criterion is in excellent agreement with experimental findings: successful materials exhibit a cubic crystal structure and more than ~ 4.1 valence electrons per atom. On the other hand, alloys that exhibit the chalcopyrite structure and only four valence electrons per atom are not suitable for phase change recording.

In conclusion, it was shown that materials that exhibit a cubic crystal structure may imply a pronounced change in density and optical contrast between the amorphous and crystalline phase and may therefore be suitable for phase change recording. This is caused by p-bonding and is predictable from N_{sp}, the number of valence electrons per atom. This is a criterion that phase change alloys have to fulfill in order to work, and may be able to find new and possibly superior phase change alloys.
However, apart from that, the knowledge of the recrystallization mechanism is also of significant importance for the development of new alloys. Therefore, studies of the crystallization kinetics as a function of recrystallization mechanism are given in the next section.

3. SPATIALLY RESOLVED CRYSTALLIZATION KINETICS

To meet future requirements for multi-media applications, the data transfer rate of phase change media must further be increased. This can only be achieved by accelerating the time-limiting factor, which is the re-crystallization of an amorphous mark in crystalline surrounding. Therefore, it is essential to understand the mechanisms of re-crystallization of phase change materials. Two mechanisms of re-crystallization depending on the composition of the alloy have been observed. For instance, AgIn-doped Sb_2Te (the material of choice in DVD-RW) re-crystallizes by the growth of the crystalline phase from the rim of the amorphous mark[8]. In contrast, $Ge_4Sb_1Te_5$ and $Ge_2Sb_2Te_5$ (the latter is the material of choice in DVD-RAM) re-crystallize by nucleation and subsequent growth of crystals inside the amorphous mark[9]. The atomistic basis for this difference is still not clearly understood. Even though several research groups have assumed that these alloys differ in their crystal nucleation rate and crystal growth velocity, systematic measurements of these two quantities as a function of temperature for *both* re-crystallization mechanisms have to the best of our knowledge not been performed. Therefore, in many modeling studies of re-crystallization the fitting parameters have no direct

experimental justification[10,11,12]. Additional difficulties arise because the glass transition temperature T_g is usually accompanied by a discontinuity in the temperature derivative of several physical quantities[13,14,15]. Therefore, crystallization parameters (in particular activation energies) determined experimentally from the easily accessible amorphous phase (below T_g) cannot be extrapolated into the undercooled liquid (above T_g). Only experimental data collected above T_g are useful for the simulation and understanding of the re-crystallization process of phase change media under operating conditions. Therefore, there is a strong demand for systematic measurements of the nucleation and growth rates in the regime of the undercooled liquid.

Transmission electron microscopy (TEM) is a powerful tool to study crystallization of thin films of amorphous Te alloys[16]. Isothermal nucleation and growth rates as a function of temperature have been measured by in-situ TEM for $Ge_2Sb_2Te_5$ [17,18] by counting crystals and measuring their change in size. This method, however, has two major uncertainties: first, precise temperature control (which is essential due to the strong temperature dependence of thermally activated processes) is often very difficult[17], and second, the electron beam significantly influences crystallization[19,20].

In this manuscript we present a different approach to the determinations of nucleation and growth rates, which avoids these two difficulties. Due to the mass density increase upon crystallization, which induces a reduction in film thickness on the order of 5% [21,22], crystals could be directly observed as depressions in the amorphous film with a Digital Instruments 3100 atomic force microscope (AFM) in TappingMode™. Three compositions, $Ag_{0.055}In_{0.065}Sb_{0.59}Te_{0.29}$ (hereafter AgInSbTe), $Ge_4Sb_1Te_5$ and $Ge_2Sb_2Te_5$, were investigated. These films (thickness: 30 nm) were prepared by direct current magnetron sputtering on 640 µm thick Si (100) wafers. The background pressure was approximately 10^{-6} mbar and the working pressure during sputtering in Ar ambient was 7×10^{-3} mbar. The sputtering power was 100 W. The deposition rate was approximately 0.5 nm/s and the target-substrate distance 5 cm. As determined from X-ray diffraction (XRD) and TEM measurements, the structure of the as-deposited films was entirely amorphous, i.e. no evidence of partial crystallization during deposition could be observed. These samples were alternately ex-situ annealed and scanned in the AFM. A specific sample was always annealed at the *same* temperature and rescanned in the AFM at the *same* microscopic location (this was possible by scratching the film with a fine needle and using the optical microscope attached to the AFM to relocate the site). Using several samples, these annealing/rescanning cycles were performed at several temperatures, 5°C apart (experimentally observable ranges: 140°C - 185°C for AgInSbTe and $Ge_4Sb_1Te_5$; and 115°C - 145°C for $Ge_2Sb_2Te_5$). The isothermal crystal growth velocity was determined from two subsequent AFM scans from the ratio of the increase in crystal radius (average over 10-20 crystals) and the annealing time.[23] Depending on the temperature, between 2 and 9 annealing/rescanning cycles were performed. This enabled us to establish the time dependence of the growth velocity for up to 8 stages of the transformation. Counting, as a function of time, the number of crystals per unit area gave the isothermal crystal nucleation rate.

For the lower temperatures, where crystallization proceeded on a timescale of hours to minutes, annealing was performed in a high-precision furnace of a Perkin Elmer Pyris 1 differential scanning calorimeter (DSC) in an argon atmosphere [furnace dimensions: 9 mm diameter, 4 mm height (cylindrical), temperature uncertainty: less than 0.1°C, heating/cooling rate: 50 K/min, no overshoot]. For the higher temperatures, where crystallization proceeded on a timescale of about a minute to a few seconds, the sample was immersed manually into safflower oil of the desired temperature and subsequently quenched into room temperature ethylene glycol. The sample (8mm x 4mm) was held by a copper wire (0.5mm diameter), which was coiled two or three times around the sample. The oil was stirred continuously, and its temperature was measured by a mercury thermometer (temperature uncertainty: less than 0.5°C). Oil residues on the sample were cleaned off with an isopropanol-soaked soft cloth after each anneal.

Figure 6 shows a selection of two AFM scans for two temperatures per alloy. Scans on $Ge_4Sb_1Te_5$ and $Ge_2Sb_2Te_5$ look qualitatively similar. The scans on AgInSbTe differ from those on the GeSbTe alloys in two major respects: First, at a given time and temperature (represented by a single AFM scan), the crystal diameter distribution is rather sharp for AgInSbTe but broad for the GeSbTe alloys. Since the isothermal crystal growth velocity of neighboring crystals was observed to be identical, this implies that all (heterogeneous) nucleation sites are approximately simultaneously exhausted for AgInSbTe. In contrast, the isothermal nucleation rate remains non-zero at all times for the GeSbTe alloys. Second, the total number of crystals per unit area, which would be observed after complete crystallization of the sample surface, increases with increasing temperature for the GeSbTe alloys, but adopts a temperature-independent value of

$(5.0 \pm 0.3)\ \mu m^{-2}$ for AgInSbTe. This behavior was observed in the entire temperature range investigated. Cross-sectional TEM[24,25] shows that crystals nucleate only heterogeneously at the (naturally oxidized) film surface. Heterogeneous nucleation at the film-substrate interface did not occur.

Over the entire temperature range investigated, the isothermal crystal growth velocity was observed to be time-independent for all three alloys. This implies that the growth was interface-controlled (in contrast to diffusion-controlled growth, where the position of the interface is proportional to the square root of time)[26]. Figure 7 is an Arrhenius plot of the crystal growth velocities, u. Growth velocities of AgInSbTe and $Ge_4Sb_1Te_5$ are similar at a given temperature. Crystal growth is thermally activated. The fitting parameters obtained from the Arrhenius fits are given in Table II. For $Ge_2Sb_2Te_5$, our value of $E_u = (2.35 \pm 0.05)$ eV agrees well with that of Privitera et al.[18] [$E_u = (2.4 \pm 0.3)$ eV] but differs slightly from that of Ruitenberg et al.[17] [$E_u = (1.6 \pm 0.6)$ eV]. Both literature values were obtained in about the same temperature range by in-situ TEM. The deviation between the latter value and ours may be due to the large temperature uncertainty of ±10°C reported in Ref. 17. For AgInSbTe and $Ge_4Sb_1Te_5$, to the best of our knowledge, no values of E_u have been reported in the literature.

For all alloys, E_u is significantly higher than the value for the isoconfigurational viscosity, E_η , which was measured[27] between 60°C and 100°C (Table II). Since the transport coefficients for viscous flow, diffusion and crystal growth are proportional, their activation energies should be the same. However, as the glass transition temperature T_g is usually accompanied by a discontinuity in activation energies[13-15], the data presented in Fig. 7 appear to be taken *above* the glass transition temperature T_g, that is, in the undercooled liquid state: T_g depends on the timescale of the experiment[13-15] and should be significantly lower in these isothermal experiments than the values of T_g ~150° C-190° C determined in the earlier scanning experiments[28]. In contrast, the measurements presented in Ref. 27 were performed far below T_g in the amorphous phase. That the crystal growth velocity in Fig. 7 is time-independent points in the same direction: only in the amorphous phase, but not in the undercooled liquid, would a time dependence of the atomic transport rates be expected due to structural relaxation[14,15,27].

In conclusion, we have demonstrated that the combination of an AFM and a high-precision furnace provides an accurate method to determine isothermal crystallization parameters as a function of time and temperature. Our method should be generally applicable to thin films that exhibit heterogeneous crystal nucleation at the film surface and a density change upon crystallization of a few percent. The difference in nucleation behavior between AgInSbTe and the GeSbTe alloys was observed to be much more pronounced than the difference in growth characteristics (all three alloys exhibited interface-controlled growth and similar activation energies E_u between 2.3 and 2.9 eV). This suggests that the different re-crystallization mechanisms observed upon laser heating[8,9] can be ascribed to the significant difference in crystal nucleation behavior rather than to the smaller difference in crystal growth velocity. The continuous nucleation observed in the GeSbTe alloys is reflected in the nucleation-dominated re-crystallization of laser-heated amorphous marks[9]; the saturation of nucleation observed in AgInSbTe corresponds to the growth-dominated re-crystallization of the marks[8].

Table I. Some successful and unsuccessful PC materials and their crystal structures. The average valence electron number N_{sp} was taken from various publications listed in Ref. 7.

	Material	Structure	N_{sp}
Successful samples	GeTe	Rocksalt	5.00
	$GeSb_2Te_4$	Rocksalt (metastable)	4.75
		Hexagonal (stable)	5.43
	$Ge_2Sb_2Te_5$	Rocksalt	4.80
	$Ge_4Sb_1Te_5$	Rocksalt	5.10
	In_3SbTe_2	Rocksalt	4.30
	$AgSbTe_2$	Rocksalt	4.50
	$AuSbTe_2$	Rocksalt	4.50
	$Au_{25}Ge_4Sn_{11}Te_{60}$	Cubic	4.45
	$Ag_3In_4Sb_{76}Te_{17}$	Cubic	4.93
Unsuccessful samples	$AgInTe_2$	Chalcopyrite	4.00
	$AuInTe_2$	Chalcopyrite	4.00

Table II. Fitting parameters of the Arrhenius fits [$\ln(u) = \ln(u_0) - E_u/(k_B T)$] in Fig. 7. Activation energies for the isoconfigurational viscosity E_η are given for comparison.

Alloy	$\ln(u_0)$ (u_0 in pm/s)	E_u (eV)	E_η [a] (eV)
AgInSbTe	84.0 ± 1.2	2.90 ± 0.05	1.33 ± 0.09
$Ge_4Sb_1Te_5$	79.2 ± 0.8	2.74 ± 0.03	1.94 ± 0.09
$Ge_2Sb_2Te_5$	72.0 ± 1.5	2.35 ± 0.05	1.76 ± 0.05

[a] From Ref. 27.

[1] H. J. Borg, M. v. Schijndel, J. C. N. Rijpers, et al., Jpn. J. Appl. Phys., Part 1 **40**, 1592 (2001).
[2] H. Iwasaki, M. Harigaya, O. Nonoyama, et al., Jpn. J. Appl. Phys., Part 1 **32**, 5241 (1993).
[3] R. Detemple, D. Wamwangi, M. Wuttig, and G. Bihlmayer, Appl. Phys. Lett. **83**, 2572 (2003).
[4] J.P. Perdew, K. Burke, and M. Ernzerhof, Phys. Rev. Lett. **77**, 3865 (1996).
[5] E. Wimmer, H. Krakauer, M. Weinert, and A.J. Freeman, Phys. Rev. B **24**, 864 (1981).
[6] D. Wamwangi, R. Detemple, H.-W. Wöltgens, M. Wuttig, and X. Zhang, J. Appl. Phys. **95**, 7567 (2004).
[7] M. Luo and M. Wuttig, Adv. Mater. **16**, 439 (2004).
[8] H.J. Borg, M. van Schijndel, J.C.N. Rijpers et al., Jpn. J. Appl. Phys. **40**, 1592 (2001).
[9] J.H. Coombs, A.P.J.M. Jongenelis, W. van Es-Spiekman, et al., J. Appl. Phys. **78**, 4918 (1995).
[10] C. Peng, L. Cheng, and M. Mansuripur, J. Appl. Phys. **82**, 4183 (1997).
[11] A.C. Sheila and T.E. Schlesinger, J. Appl. Phys. **91**, 2803 (2002).
[12] E.R. Meinders, H.J. Borg, M.H.R. Lankhorst, et al., J. Appl. Phys. **91**, 9794 (2002).
[13] W. Kauzmann, Chem. Rev. **43**, 219 (1948).
[14] F. Spaepen, in *Physics of Defects*, edited by R. Balian, M. Kleman, and J.-P. Poirier (Les Houches Lectures XXXV, North-Holland, Amsterdam, 1981), pp. 136-174.
[15] F. Spaepen and D. Turnbull, Ann. Rev. Phys. Chem. **35**, 241 (1984).
[16] M. Libera and M. Chen, J. Appl. Phys. **73**, 2272 (1993).
[17] G. Ruitenberg, A.K. Petford-Long, and R.C. Doole, J. Appl. Phys. **92**, 3116 (2002).
[18] S. Privitera, C. Bongiorno, E. Rimini, et al., Mat. Res. Soc. Symp. Proc. **803**, HH 1.4 (2004).
[19] M. Libera, Appl. Phys. Lett. **68**, 331 (1996).
[20] B.J. Kooi, W.M.G. Groot, and J.Th.M. De Hosson, J. Appl. Phys. **95**, 924 (2004).
[21] V. Weidenhof, I. Friedrich. S. Ziegler, and M. Wuttig, J. Appl. Phys. **86**, 5879 (1999).
[22] T.P. Leervad Pedersen, J. Kalb, W.K. Njoroge, D. Wamwangi, M. Wuttig, and F. Spaepen, Appl. Phys. Lett. **79**, 3597 (2001).
[23] J. Kalb, F. Spaepen, and M. Wuttig, Appl. Phys. Lett. **84**, 5240 (2004).
[24] T.H. Jeong, M.R. Kim, H. Seo, et al., J. Appl. Phys. **86**, 774 (1999).
[25] J. Kalb, C.-Y. Wen, F. Spaepen, and M. Wuttig, unpublished.
[26] J. W. Christian, *The Theory of Transformations in Metals and Alloys* (Pergamon Press, North-Holland, Amsterdam, 2nd ed., 1975).
[27] J. Kalb, F. Spaepen, T.P. Leervad Pedersen, and M. Wuttig, J. Appl. Phys. **94**, 4908 (2003).
[28] J. Kalb, F. Spaepen, and M. Wuttig, J. Appl. Phys. **93**, 2389 (2003).

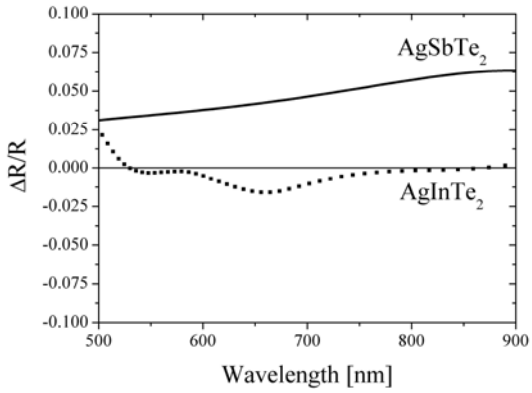

Fig. 1: Normalized reflectance change for both alloys determined from 500 nm up to 900 nm. The dotted line denotes the contrast for a 60 nm thin $AgInTe_2$ film on a glass substrate as function of the wavelength, while the same layer stack, where $AgInTe_2$ is replaced by $AgSbTe_2$, yields the solid line.

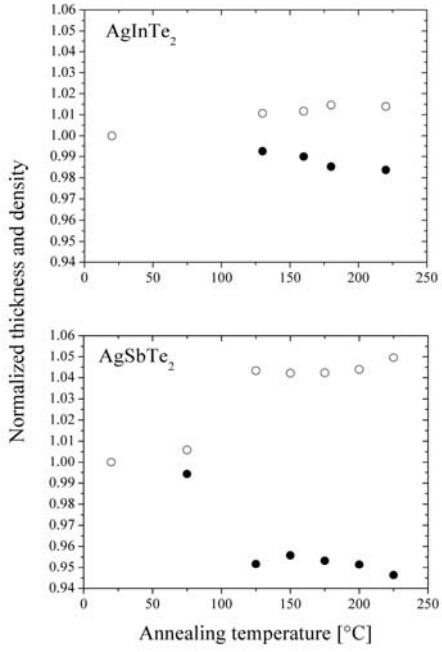

Fig. 2: Thickness change upon furnace crystallization for both ternary alloys as a function of annealing temperature as determined by x-ray reflectivity measurements. The thickness is normalized with respect to the as deposited amorphous film, which is 56 nm for $AgInTe_2$ and 57 nm for $AgSbTe_2$. The upper diagram shows the small density change of $AgInTe_2$, which is only 29% relative to the density change of the $AgSbTe_2$ alloy.

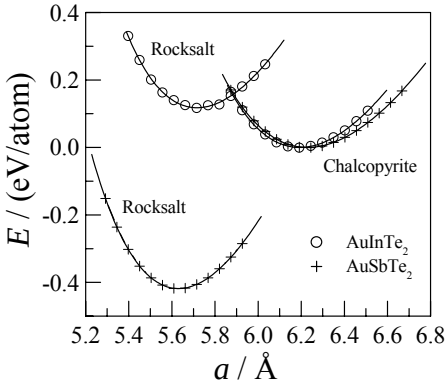

Fig. 3: Dependence of the total energy per single atom E on lattice parameter a for rocksalt and chalcopyrite crystal structure for materials $AuInTe_2$ and $AuSbTe_2$. Open circles and crosses are DFT calculation results, and solid curves are least-square fits of Murnaghan equation of state. The stable structure for $AuInTe_2$ is the chalcopyrite structure and that for $AuSbTe_2$ is the rocksalt structure. The energy of the chalcopyrite structure is set as the energy reference.

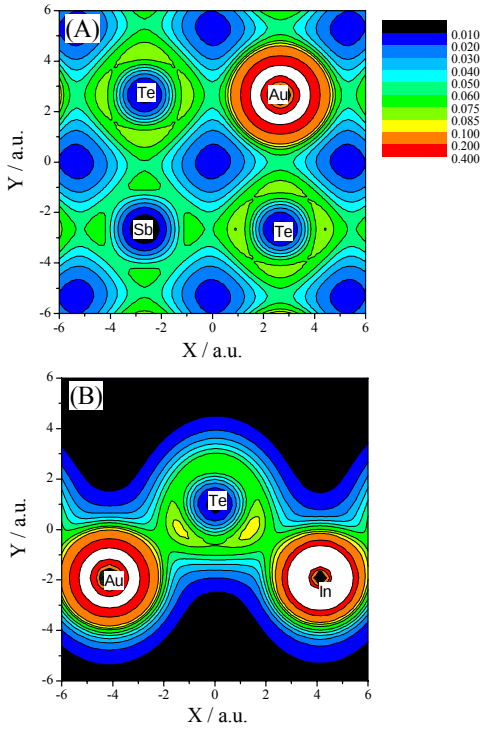

Fig 4. The electronic density on the 001 plane for $AuSbTe_2$ with rocksalt structure (A) and the 110 plane for $AuInTe_2$ with chalcopyrite structure (B). We consider $5d^{10}6s^1$, $4d^{10}5s^25p^1$, $5s^25p^3$, $5s^25p^4$ electrons of atoms Au, In, Sb and Te, respectively as valence electrons for the pseudopotential used in the DFT calculation. The electronic density is in unit of $e/a.u.^3$.

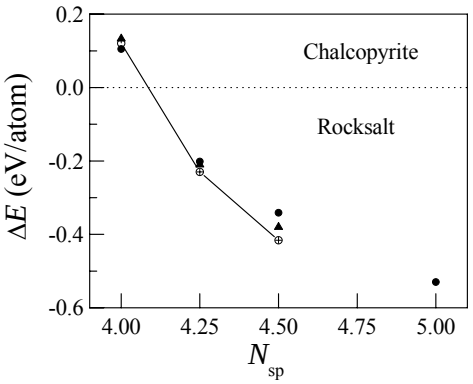

Fig. 5 (top): Plot of the energy difference per single atom ΔE for different average valence electron number N_{sp}. Open circles (○) represent Au(In,Sn,Sb)Te_2; Solid triangles (▲) represent Ag(In,Sn,Sb)Te_2; Crosses (+) represent Cu(In,Sn,Sb)Te_2; Solid circles (●) represent $AuGaTe_2$, $AuGeTe_2$, $AuAsTe_2$, and $InSbTe_2$, respectively. Solid line is the link for Au series of alloys.

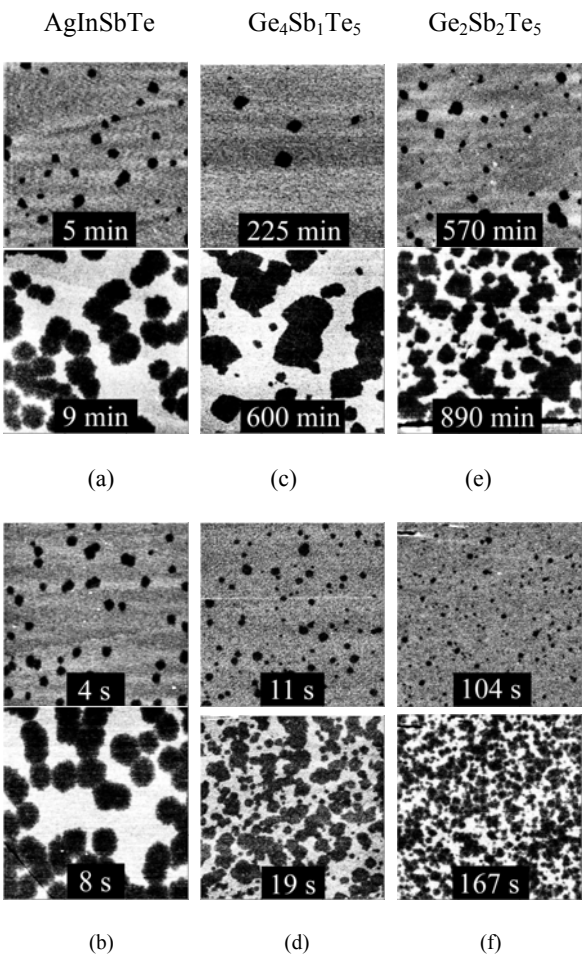

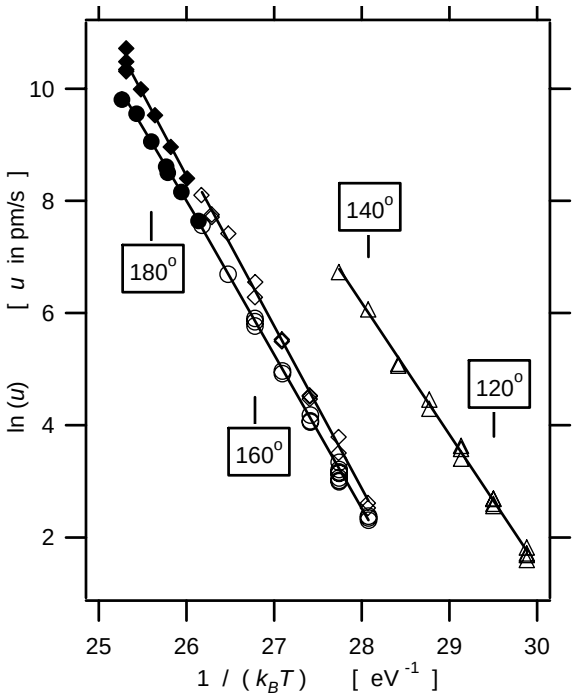

Fig. 7 (top). Crystal growth velocity u as a function of temperature T. Open squares: AgInSbTe, DSC anneal. Full squares: AgInSbTe, Immersion anneal. Open circles: $Ge_4Sb_1Te_5$, DSC anneal. Full circles: $Ge_4Sb_1Te_5$, Immersion anneal. Open triangles: $Ge_2Sb_2Te_5$, DSC anneal. For $Ge_2Sb_2Te_5$, the crystal density was too high to allow measurements using immersion anneals. The error bars on the velocity are on the order of the symbol size. For AgInSbTe and $Ge_4Sb_1Te_5$, DSC and immersion anneal data were fitted separately, and the fitting parameters were subsequently averaged. These averaged values (Table II) are less sensitive to possible small systematic errors in the temperature calibration of the two annealing methods.

Fig. 6 (left). AFM scans (dimensions: 3 μm by 3 μm): Crystals (dark, height: -2 nm) are visible in amorphous surrounding (bright, zero height). (a) AgInSbTe, 160°C. (b) AgInSbTe, 185°C. (c) $Ge_4Sb_1Te_5$, 140°C. (d) $Ge_4Sb_1Te_5$, 180°C. (e) $Ge_2Sb_2Te_5$, 115°C. (f) $Ge_2Sb_2Te_5$, 145°C. All times indicated are *total* times (including times of preceding anneals). Note that each crystal in (a) and (b) is present in both top and bottom images.